Open Research Online

The Open University's repository of research publications
and other research outputs

The impact of radiation damage on photon counting with an EMCCD for the WFIRST-AFTA coronagraph

Conference Item

oro.open.ac.uk

The impact of radiation damage on photon counting with an EMCCD for the WFIRST-AFTA coronagraph

Nathan Bush[a] [*], David Hall[a], Andrew Holland[a], Ross Burgon[a], Neil Murray[a], Jason Gow[a], Matthew Soman[a], Douglas Jordan[b], Richard Demers[c], Leon K. Harding[c], Michael Hoenk[c], Darren Michaels[c], Bijan Nemati[c] and Pavani Peddada[c]

[a] Centre for Electronic Imaging, The Open University, Walton Hall, Milton Keynes, MK7 6AA, UK

[b] e2v Technologies plc, Waterhouse Lane, Chelmsford, Essex CM1 2QU, UK

[c] Jet Propulsion Laboratory, 4800 Oak Grove Drive, Pasadena, CA 91109-8099, US

ABSTRACT

WFIRST-AFTA is a 2.4m class NASA observatory designed to address a wide range of science objectives using two complementary scientific payloads. The Wide Field Instrument (WFI) offers Hubble quality imaging over a 0.28 square degree field of view, and will gather NIR statistical data on exoplanets through gravitational microlensing. The second instrument is a high contrast coronagraph that will carry out the direct imaging and spectroscopic analysis of exoplanets, providing a means to probe the structure and composition of planetary systems.

The coronagraph instrument is expected to operate in low photon flux for long integration times, meaning all noise sources must be kept to a minimum. In order to satisfy the low noise requirements, the Electron Multiplication (EM)-CCD has been baselined for both the imaging and spectrograph cameras. The EMCCD was selected in comparison with other candidates because of its low effective electronic read noise at sub-electron values with appropriate multiplication gain setting. The presence of other noise sources, however, such as thermal dark signal and Clock Induced Charge (CIC), need to be characterised and mitigated. In addition, operation within a space environment will subject the device to radiation damage that will degrade the Charge Transfer Efficiency (CTE) of the device throughout the mission lifetime.

Here we present our latest results from pre- and post-irradiation testing of the e2v CCD201-20 BI EMCCD sensor, baselined for the WFIRST-AFTA coronagraph instrument. A description of the detector technology is presented, alongside considerations for operation within a space environment. The results from a room temperature irradiation are discussed in context with the nominal operating requirements of AFTA-C and future work which entails a cryogenic irradiation of the CCD201-20 is presented.

Keywords: WFIRST-AFTA, coronagraph, EMCCD, radiation damage, photon-counting, Charge Transfer Efficiency

[*] Corresponding author.
Email: nathan.bush@open.ac.uk

1. INTRODUCTION: THE WFIRST-AFTA CORONAGRAPH

The identification and characterisation of extrasolar planets has been of growing interest for the astronomical community throughout the past decade. At the time of writing, over 1000 separate systems have been identified and some studies have found that planetary systems are widely distributed throughout our galaxy.[1] The ability to detect and characterise such systems has also advanced considerably within the same time-scales. Techniques such as transit photometry and Doppler spectroscopy have been highly successful[2,3] and the development of advanced Adaptive Optics (AO) systems has further improved angular resolution for ground based observatories.

Despite these advances, the majority of exoplanets still have their presence confirmed indirectly through the effect of their presence on the parent star. Such discoveries are biased to large planets with short orbital periods which do not represent the entire population. Although many smaller and longer period planets have been discovered,[4] these targets are typically too faint for detailed atmospheric characterisation within the time-scales of space based missions. The direct detection of exoplanets, through either direct imaging or spectroscopy, can allow for significantly more detailed characterisation. In addition, planets discovered through direct imaging can exhibit longer orbital periods and are a probe of planetary structure and composition in the absence of high irradiation from the parent star. Direct imaging techniques therefore have the potential to uncover and characterise a population of exoplanets both with properties similar to those within our own solar system and some which vastly differ, including Cold-Jupiters, Mini-Neptunes and Super-Earths.[5]

Direct detection is difficult since the light reflected from the target planet is orders of magnitude fainter than the parent star. A coronagraph is an optical system specifically suited to such an environment, creating high contrast within a small working angle through both occultation of the parent star and suppression of the resulting diffraction pattern. Achieving the required contrasts for the imaging of fainter exoplanets remains challenging, but will be absolutely necessary to further understand the formation of planetary systems and extensively characterise planetary atmospheres. The advancement of high contrast imaging in space was therefore the number 1 priority at medium scale for NASA in the 2010 decadal survey. The WFIRST-AFTA coronagraph (AFTA-C) is a direct response to this challenge, and will represent a significant advancement in the field. Contrasts of up to 10^{-9} will be possible, following post-processing, and the instrument will provide the first direct images of planets surrounding our nearest stellar neighbours that may be similar to our own giant planets.[5] The science goals of the mission require every aspect of the instrument to be appropriately selected, including the instrument camera systems. The e2v CCD201-20 EMCCD has been baselined as the detector for each of the instrument cameras due to the low noise the detector can provide when operating under low-flux conditions.

Figure 1: WFIRST-AFTA mission concept.[5]

2. EM-CCD TECHNOLOGY & THE CCD201-20

The Electron Multiplying CCD (EMCCD) is a variant of traditional CCD technology that is well suited to low-light-level applications.[6] An image area, serial register and output node are all present that are of conventional design (Figure 2). The main modification is the inclusion of a multiplication register; an array of elements that are designed to allow signal carriers to experience high electric fields. The high electric fields accelerate the carriers to energies sufficient for the generation of additional electron-hole pairs from the silicon lattice in a process known as impact ionisation.

In practise this is achieved with a 4-gate structure where two of the electrodes are customised to generate a region of high field. The barrier phase, ϕDC, is held at a low fixed voltage during operation. The high-voltage phase (Rϕ2HV) can have a timed, high voltage pulse applied to establish the region of high field. The remaining two electrodes (Rϕ1, Rϕ3) operate at standard device potentials and act to transfer charge from one multiplication element to the next. Appropriate clocking allows the signal to be passed from the previous element, experience multiplication, and then be passed to the following element where the process repeats (figure 3).

The multiplication per element-to-element transfer is typically of the order 1-1.5% and is a non-linear function of the potential difference between ϕDC and Rϕ2HV. Multiple consecutive elements mean that large multiplication gains can be achieved at relatively modest operating voltages. Typically there are over 500 multiplication elements on a device, and gains of ×1000 can be achieved with voltages for Rϕ2HV in the range 40-46 V relative to ϕDC voltages in the range 3-5 V. A previously small signal can therefore be amplified to a level where the read noise introduced by the output amplifier is no longer significant, lowering the effective read noise floor to sub-electron levels.
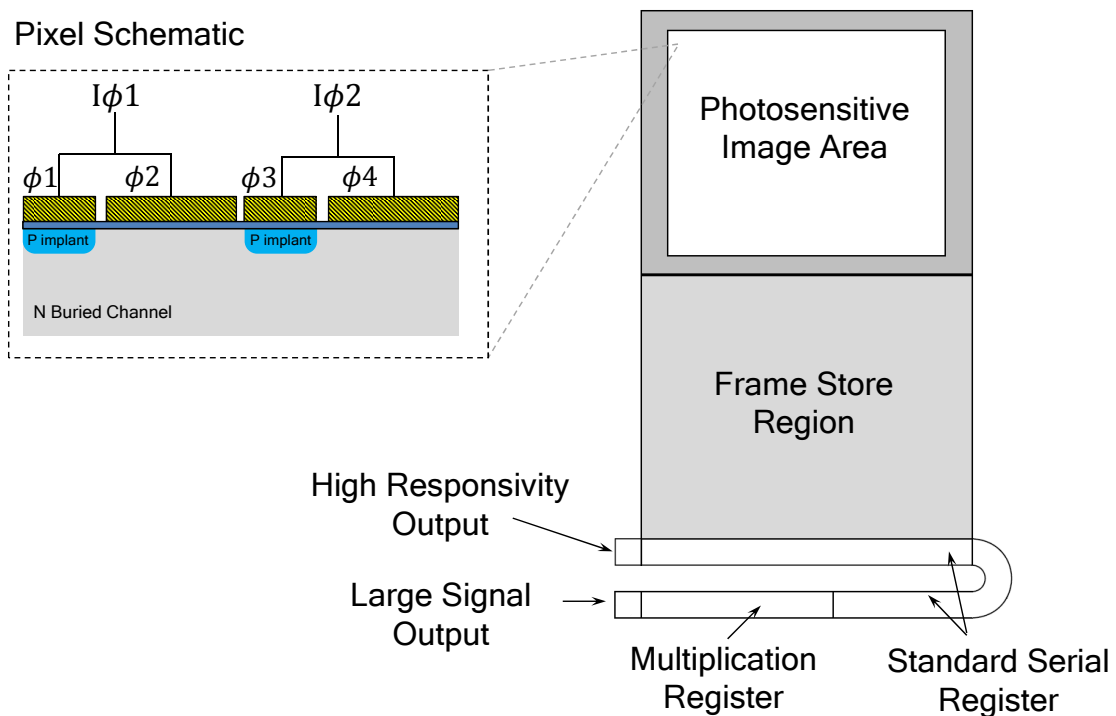

Figure 2: Example EMCCD schematic, adapted from the CCD201-20 datasheet. The pixel schematic is shown perpendicular to the direction of transfer for clarity.[7]
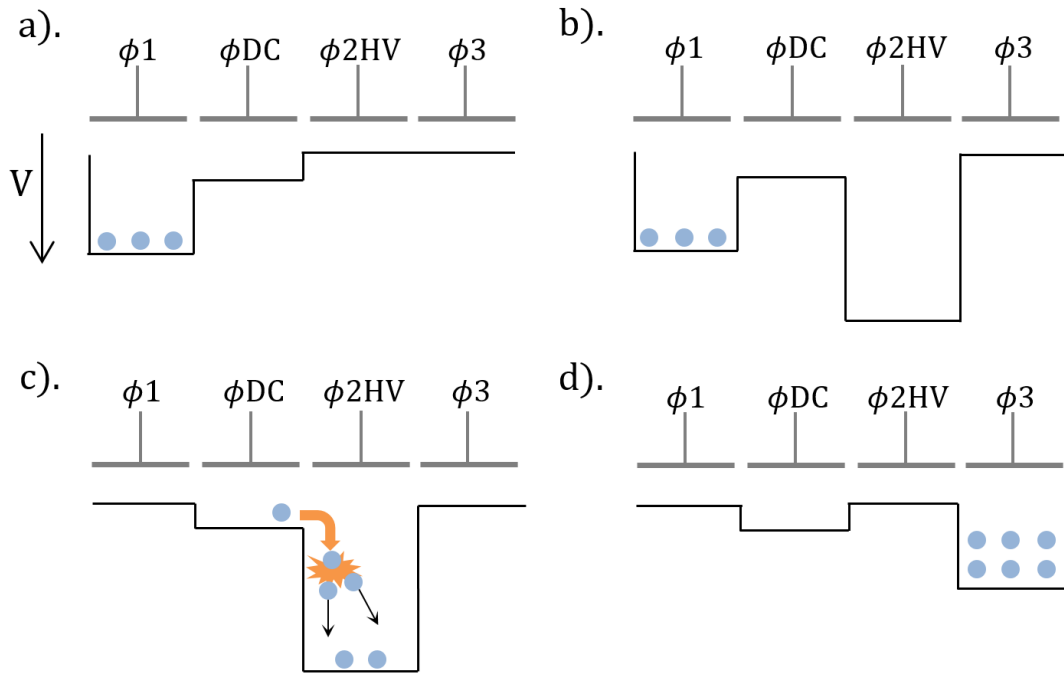
3

Figure 3: Example EMCCD clocking sequence. The ϕDC phase prevents the motion of charge while the high field is established (b). Impact ionisation occurs as the charge is transferred between ϕDC and ϕ2HV (c). The signal can then be transferred to the following multiplication element.

Since its introduction the technology has found a wide range of applications, including use in the military,[8] biomedical imaging[9] and ground based astronomy.[10] The WFIRST-AFTA coronagraph shall be the first instrument to implement the technology for a large scale space mission. The specific sensor baselined is the CCD201-20, a commercially available EMCCD sensor manufactured by e2v technologies. The CCD201-20 has a 1k×1k image format that is back-thinned for high Quantum Efficiency (QE). Two separate outputs are present that allow operation as either a standard CCD or EMCCD as required. The image and store pixels have additional implants introduced during manufacture that allow 2-phase clocking and operation in either Inverted or Non-Inverted Mode (Figure 2).

The selection of this detector for use on WFIRST-AFTA was based upon a comprehensive trade study that identified the key strengths of EMCCD technology compared to competing technologies for low light imaging, including its high quantum efficiency in the AFTA-C wavebands (approximately 660-890 nm) and the low possible total noise floor.[11] Achieving the lowest possible noise is essential for the AFTA-C application, and requires careful optimisation of the EMCCD to the specific operating environment alongside a detailed understanding of each of the dominant noise sources and how they can each be minimised.

2.1 Noise sources for EM-CCDs

For the AFTA-C application, appropriate multiplication gain will reduce the read noise to sub-electron levels where it will be longer be a significant contributor to the total noise floor. With the elimination of read noise, three noise sources remain to be considered; the noise due to the multiplication process, thermal dark signal and Clock Induced Charge (CIC). Each of these sources contribute differently depending upon how the device is operated.

1. **The Excess Noise Factor (ENF)**. The multiplication process is inherently stochastic due to the statistical nature of carrier generation within the EM register and adds additional noise to the system. For imaging of optical photons, the noise introduced by this process is best described as a factor increase over the Poisson noise, termed the Excess Noise Factor (ENF), and has been shown to tend to $\sqrt{2}$ for a large number of elements at high multiplication gain.[12] When used for X-ray detection, the excess noise factor takes a different form, described in detail by Tutt *et al.*[13] At large signal levels the ENF translates to an effective halving in the QE of the detector. However, for sufficiently low optical signal levels (≤ 20 e$^-$/pix/s), some reduction in the ENF is possible through post-processing techniques.[14] Operation in "binary mode", where the output of each pixel is assessed against a fixed threshold (commonly 5σ above the total noise floor) can reduce the ENF to unity, permitting the detection of single photons.[15] In summary there are three distinct operation regimes where the total noise of the system may vary through use of the on-chip multiplication gain, dependent upon the incident flux, I:

   i $I \geq 20$ e$^-$/pix/s - The high flux regime. The use of high multiplication gain introduces a factor increase of $\sqrt{2}$ over Poisson noise. (Often referred to as "Analogue Gain Mode").

   ii $1 \leq I \leq 20$ e$^-$/pix/s - The low flux regime. Some recovery of the ENF is possible through post processing techniques.[12]

   iii $I \leq 1$ e$^-$/pix/s - The photon counting regime. Appropriate thresholding makes the ENF effectively irrelevant.

   Preliminary studies have shown that the coronagraph instrument would benefit from increased signal to noise through operation in either the low flux regime or photon counting regime, with the greatest benefit seen through photon counting. Operation in photon counting mode is therefore the nominated operating mode of the device.[5] Photon counting mode eliminates the contribution of the ENF such that thermal dark signal, and clock induced charge become the limiting contributors to noise.

2. **Thermal Dark Signal** encompasses signal thermally excited into the conduction band from either bulk or surface states of the detector which is then collected by the the device during operation. The surface component typically dominates the bulk component by at least an order of magnitude but can be suppressed through operation in Inverted Mode (IMO), whereby the raising of the substrate voltage with respect to the image clocks causes the semiconductor-insulator interface to become flooded with holes, suppressing electron emission from interface traps. The remaining bulk state contribution to dark current can be significantly reduced by cooling the detector. For the baseline design of the AFTA coronagraph, the nominal operating temperature is 165.15K (-108°C) where dark current levels of the order of 10^{-4} e$^-$/pix/s have been measured in IMO.[16]

3. **Clock Induced Charge** (CIC) is signal generated by the process of clocking charge through the device. It is generally accepted that it is caused by minority carriers experiencing high electric fields as a phase is driven out of inversion, generating additional electron hole pairs through impact ionisation.[17] CIC has an exponential dependence on the applied clock swing between successive phases of the device, with higher clock swings corresponding to higher CIC. It also has a dependence on the clocking frequency, where faster pixel rates give rise to lower measured CIC. Since the mechanism is dependent on the motion of holes within N-channel CCDs, operation in IMO has been linked to significantly higher levels of CIC when compared to NIMO. It has, however, been shown that low levels of CIC similar to those measured in NIMO can be achieved when operating the device in IMO through customised clocking of the device.[18]

The desired mode of operation, namely either IMO or NIMO, is a balance of the dark signal accumulated during frame integration and the clock induced charge generated by the readout process. It follows that as the integration time increases IMO operation becomes increasingly favoured, since the dark current component will eventually dominate. For the AFTA-C application, integration times are expected to be of the order 100-200 s.[5] In this regime noise due to dark signal is expected to become the dominant component, so long as CIC can be reduced to levels similar to those shown in Daigle et al.[16] Based on this information, operation in IMO is planned since it will allow the lowest possible noise when operating in photon counting mode.

2.2 EM-CCDs in a radiation environment

Operation of the device in both IMO and photon counting mode has the potential to provide a significant benefits for AFTA-C when compared to traditional CCD technology.[11] What remains to be considered is the degradation of the device throughout the mission lifetime; the device will be subject to the radiation environment and the ionising and non-ionising displacement damage that is associated with it. This radiation damage will have an effect on certain performance characteristics, including dark current and Charge Transfer Efficiency (CTE). Other performance metrics such as the effective read noise, multiplication gain and clock induced charge may also be affected and require consideration.

Several investigations have been performed concerning the radiation hardness of EMCCD technology. Particular attention has been paid to the effects of proton displacement damage and ionising damage on the multiplication gain register, since this is the key design difference when compared to a standard CCD. Of note are the investigations performed by Smith et al.[19] and Hadwen et al.,[20] who investigated the effects of proton displacement damage and gamma radiation respectively. The proton irradiation campaign of Smith et al. comprised of the irradiation of 95 CCD-97s with a 10 MeV equivalent fluence of 2×10^{10} protons cm^{-2}. Each of the devices irradiated were said to have experienced an increase in dark current and bright pixel population that was consistent with standard CCD devices and no complete device failures due to proton displacement damage were noted. The gamma irradiation campaign of Hadwen et al. was performed on two CCD-87s that were each irradiated in steps to a Total Ionising Dose (TID) of 20 krad (Si). The "global" threshold shift was measured to be 0.14 V/krad for each device, with no significant change in the multiplication gain following irradiation. A study summarised in Harding et al.[11] showed that the inclusion of a 1 mm thick glass window reduced the expected End of Life (EOL) ionising dose to the range 1-3 krad, depending on the exact shielding design used.[11] For the case of AFTA-C the TID is therefore expected to be much lower than those tested in Hadwen et al., significantly reducing the risk associated with ionising effects.[20]

The high potential difference between the ϕDC and Rϕ2HV electrodes results in a correspondingly high electric field in the insulating oxide that separates them. Ionising particles generate a track of electron-hole pairs as they pass through the oxide, which temporarily form a conductive path. If this path connects the two electrodes during operation it can cause device failure and is referred to as Single Event Gate Rupture (SEGR). An investigation into the possibility of SEGR on e2v CCD-97s[21] found that no signs of failure were present following a dose consistent with operation in L2 for 5-10 years.[22]

In summary, past investigations of the radiation hardness of EMCCD technology have provided very promising results. The effects of radiation damage are comparable to that experienced by traditional CCD sensors, which are well understood and have a rich space flight heritage. In addition, no field-enhancement effects due to the multiplication register were observed in any of the investigations, a very encouraging outcome for the AFTA-C application.

3. DISPLACEMENT DAMAGE EFFECTS ON THE CCD201-20

Although previous investigations had been performed on the radiation hardness of EMCCDs, none have been performed under operating conditions consistent with AFTA-C. The temperature and mode of operation have been shown to have a significant impact on measured performance characteristics. An investigation was therefore performed whereby two CCD201-20s were tested for key performance metrics critical for AFTA-C prior to and following irradiation to a level representative of the nominal EOL fluence for a given shielding level.

Two engineering grade CCD201-20s were procured for the investigation. 'Engineering-grade' devices have not met e2vs requirements of scientific grade but do not suffer from any significant defects. Information was provided by e2v that describes why each device had not met scientific grade (Table 1). Although the devices are considered engineering grade, the measured performance degradation following irradiation is considered to be representative of what scientific grade devices will experience.

Table 1: Devices procured for study and reasons for "engineering-grade" classification.

Device	Serial Number	Reason for 'Engineering-grade' classification
1	10091-16-19	High Dark Signal
2	11153-13-14	Bright Defects

3.1 Device Testing

The devices were tested for performance parameters that were deemed most critical to the detector requirements of AFTA-C, including dark current and CIC. The CTE was also measured using Fe^{55} X-rays (5989 eV) so that comparisons could be made to the degradation experienced by other devices in past investigations. The multiplication gain was also measured across a range of Rϕ2HV voltages.

The device bias conditions used for testing were based on those recommended by e2v,[7] with some alterations made to minimise read noise and optimise charge transfer efficiency within the multiplication register. The remaining free parameter was the Rϕ2HV voltage, adjustment of which changes the multiplication gain that signal experiences during operation. Raising the Rϕ2HV voltage higher than necessary to achieve the required effective read noise has been shown to adversely affect other performance metrics of the device, including the serial CTE of the multiplication register and the generation of CIC.[18] Based on this information, the Rϕ2HV levels were selected through measurement of the minimum required Rϕ2HV voltage to achieve the specified read noise. It is worth noting that it is the potential *difference* between RϕDC and Rϕ2HV which gives rise to the multiplication gain within the EM register. The values specified within table 3 and throughout this document (unless otherwise stated) are the applied Rϕ2HV voltages; however it is often useful to consider the effective Rϕ2HV voltage, defined as Rϕ2HV- ϕDC, when making comparisons between different devices and investigations.

Table 2: Biases used for Rϕ2HV electrode on each device. The ϕDC voltage used during testing was 5 V for both devices.

Device	Serial Number	Applied Rϕ2HV Voltage (V)
1	10091-16-19	43.4
2	11153-13-14	42.3

The same Rϕ2HV values were used for both pre- and post-irradiation testing, since any increase in Rϕ2HV voltage applied to compensate for radiation induced effects would also affect other measured performance parameters. Use of the same values pre- and post-irradiation helped ensure that any measured performance degradation was due to radiation induced effects and not due to a change in the operating conditions.

The devices were operated in IMO except for the case of readout and multiplication registers, which were operated in NIMO to reduce the level of serial CIC generated. Testing was performed under vacuum at the baselined AFTA-C operating temperature of 165K.

3.2 Room Temperature Irradiation at PSI

Irradiation of the two devices took place at the Proton Irradiation Facility (PIF) at PSI, Villigen. Switzerland. The PIF was constructed for the testing of spacecraft components under contract between ESA and PSI, and is commonly used for the radiation testing of silicon based image sensors by a number of institutions including e2v and the European Space Agency. A primary beam energy of 74 MeV was delivered by the PIF, meaning the fluence needed to be renormalized to deposit the same amount of energy into the device as a 10 MeV beam otherwise would. The Non-Ionising Energy Loss (NIEL) function, described in detail by Burke,[23] Van Lint[24] and in CCDs by Srour[25] *et al.*, allows for such a comparison to be made and was used to calculate the target fluence of 5.21×10^9 protons cm^{-2}.

Each of the devices was irradiated in different regions in order to separate the effects of displacement damage on the parallel and serial sections of the device (figure 5). Shielding was used to protect the on-chip control regions, and was made from stainless steel with a thickness of 14 mm which prevented primary beam protons reaching the control regions.

The irradiation took place on 23/02/15 and was performed at ambient temperature with the devices unbiased. Calibration performed by staff at PSI showed that the dosimetry was accurate to within 10% and that the beam uniformity over the region of each device was within this error (Figure 6). Preliminary analysis post irradiation showed that the target regions had been irradiated as expected, and that the control regions remained unaffected.
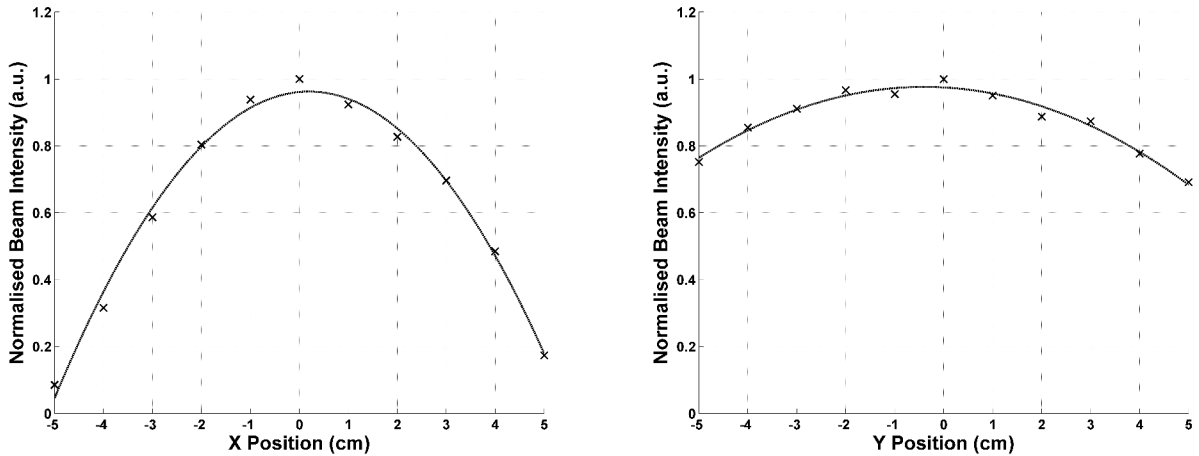

Figure 4: Beam intensity profile as measured by PSI staff immediately prior to irradiation. Although the intensity varies significantly in the x plane, the small (≤ 1 cm) target width on each chip meant the observed variation was insignificant.
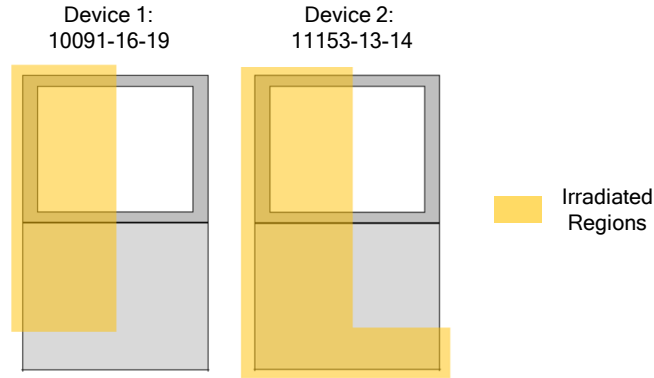
Figure 5: Irradiated regions for each device. Device 1 and Device 2 were classed as engineering grade by e2v technologies due to their high dark signal and large number of bright defects respectively.
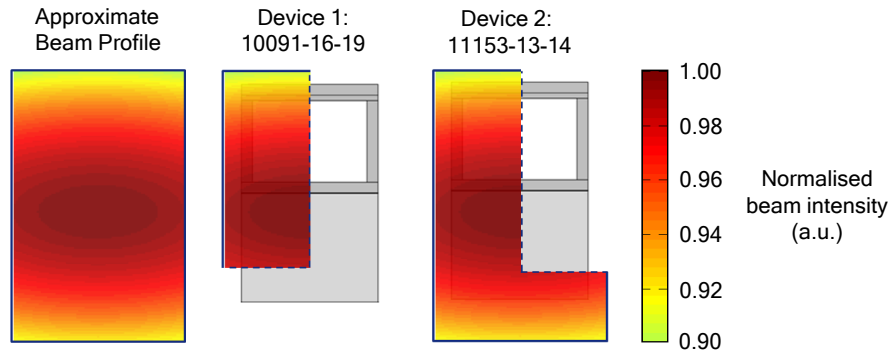

Figure 6: Beam intensity profile mapped (approximately) onto device area. The variation from end to end is $\leq 10\%$ and within the error on dosimetry.

4. RESULTS OF PRE- AND POST-IRRADIATION TESTING

Following irradiation all of the tests were repeated in order to assess the effects of displacement damage on the performance of each device. The results are summarised in table 3. Many of the characteristics following irradiation (table 3) show trends that are consistent with those observed during past investigations[19] and others provide an insight into the behaviour of the multiplication register during operation.

4.1 Multiplication Gain

The measured multiplication gain did not change within error for the case where both the parallel and serial regions of the device were irradiated (figure 9). This is consistent with that seen by Smith *et al.*, a large scale study of CCD97s, where the multiplication gain was not observed to change due to displacement damage. An interesting observation is that Device 1 showed a marked decreased in gain following-irradiation. This could not attributed to the effects of radiation since this device had its serial register shielded. Instead, this observation was thought to be due to an "ageing" effect whereby the measured multiplication gain of the device for a given $R\phi2HV$ Voltage decreases as a function of the total signal passed through the register. The phenomenon may be due to carrier trapping within the dielectric layers of the device that acts to alter the potential difference between $R\phi DC$ and $R\phi2HV$, and hence decreases the applied multiplication gain.[26,27]

9

e2v devices are preconditioned to remove the majority of ageing effects following manufacture, but some decrease can still be observed if large signals are continually passed through the multiplication register.[26] For this testing, Device 1 was operated for longer than Device 2 in order to commission the camera system and perform additional testing following irradiation, explaining why Device 1 was observed to have aged slightly while Device 2 did not. It is worth noting that since the multiplication gain is an exponential function of the applied potential only a very small change is voltage is required for the change to be measurable. A fit to the data presented in 9 showed an estimated change of approximately (0.2 ± 0.1)V. Device ageing does not represent an issue for photon counting applications since typically only small signals will be passed through the register. Thresholding techniques are also insensitive to small changes in gain so long as they are chosen appropriately.

The resistance of multiplication gain to displacement damage seen in this investigation is an encouraging result. The observation of "ageing" in Device 1 is almost certainly a side effect of the large signals passed through the register during testing and so special attention will be paid to this phenomenon in future work, described in section 5.

4.2 IMO Dark Signal

The factor increase seen in parallel IMO dark signal for each device appears consistent at approximately $\times2$ (figure 7, table 3). For displacement damage the increase in dark current is due to the generation of traps within the bulk of the device. These traps allow the thermal excitation of carriers into the conduction band which are subsequently collected within the potential well of the pixel. Device 1 and Device 2 were classed as "engineering grade" for the presence of high dark signal and a large number of bright defects respectively. The measurements shown in table 3 support this, with Device 1 exhibiting higher dark signal prior to and following irradiation.

4.3 Parallel CIC

No significant increase in parallel CIC was observed due to the effects of displacement damage for each of the devices in this study (table 3). CIC is thought to be generated by the fast movement of minority carriers to the channel stop or substrate as a phase is clocked out of inversion. The predominant trapping sites that affect CIC are therefore at the semiconductor-insulator interface, the density of which is not thought to increase significantly for the fluence and conditions used in this investigation. The measurement is therefore consistent with this description. Since CIC has been shown to be dependant on the clock rise times, amplitudes and frequencies of operation the measured values are specific to the camera system used for this study. Lower values can be achieved through operation at higher frequencies and through optimisation of clocking waveforms, however this was not a priority for this investigation since the primary aim was to observe the effect of radiation damage.

4.4 X-ray CTI

The measured X-ray CTI for each device prior to irradiation was seen to be of the order 10^{-6} and each device experienced a similar degree of degradation following irradiation (table 3, figure 8). The measured parallel CTI following irradiation is in line with other measurements made for e2v devices that were characterised at a similar temperature following irradiation to a similar fluence.[28] The serial CTI was seen to degrade by a smaller factor than the parallel CTI, a phenomenon observed in many other studies that is thought to be due to the smaller dwell time the signal packet experiences during transfer in this direction.

The X-ray CTI of the multiplication gain register was measured using the method described by Daigle *et al.*[29] whereby the increase in signal per element transfer was accounted for alongside the amount lost due to imperfect charge transfer:

$$CTE_{HV} = (1 - E_{deferred})^{1/n} \tag{1}$$

Where $E_{deferred}$ is the total amount of deferred charge and n the number of multiplication elements. The pre-irradiation X-ray CTI of the multiplication register is higher than that of the standard register (table 3). In the images of Fe^{55} X-Rays, "tails" of deferred charge could be seen for single events that were consistent with the direction of travel through the multiplication register. This has been observed by other authors when operating the devices under certain conditions.[19,30]

One cause of this effect is that if the charge handling capacity of the EM register is exceeded charge will spill into neighbouring pixels. The presence of the DC phase prior to the HV electrode means the preferred direction for blooming is towards the preceding pixel, giving rise to a tail as observed in this testing. The average Manganese K-alpha X-ray signal from an Fe^{55} source is $\approx 1616e^-$, and with the multiplication gain used for testing this corresponds to an average signal within the register of $\approx 400,000$ e$^-$. This is less than the stated charge handling capacity of $\approx 700,000$ e$^-$ for the CCD201-20[7] and so blooming due to exceeding the capacity of the register is unlikely to be the explanation.

An alternative possibility for this observation is that the high voltages used for the Rϕ2HV phase mean that the charge storage packet is in close proximity to the semi-conductor-insulator interface. Charge local to interface states has the potential to become trapped, released and then undergo multiplication when transferred through the remainder of the register, appearing as a "tail" of deferred charge. Simulations shown in previous studies have shown this may be the case and that it may be exacerbated through the use of high Rϕ2HV voltages, since the potential maximum becomes increasingly close to the interface as this bias is increased.[27]

Following irradiation, Device 1 showed a measured decrease in the CTI of the EM register. This is potentially linked to the decrease in multiplication gain that was observed for the same device. For Device 2 the X-ray CTI of the EM register was seen to degrade by approximately 1×10^{-5} - the same degradation as measured by the standard serial register. This measurement is consistent with the explanation that surface state trapping is the dominant contribution to the CTI of the EM register at these signal levels, since the same degradation due to generation of bulk states has been observed.

Table 3: Summary of results from pre- and post-irradiation testing of each device

Parameter	Device 1: Parallel Irradiation Only		Device 2: Parallel & Serial Irradiation	
	Pre-Irradiation	Post-Irradiation	Pre-Irradiation	Post-Irradiation
Multiplication Gain[(i)] (a.u)	238±7	202±6	237±8	237±8
Parallel Dark Signal (e$^-$/pixel/s)	$(7.13\pm0.49)\times10^{-5}$	$(1.22\pm0.06)\times10^{-4}$	$(3.19\pm0.50)\times10^{-5}$	$(5.75\pm0.44)\times10^{-5}$
Parallel CIC[(ii)] (e$^-$/pixel/frame)	$(4.47\pm0.24)\times10^{-2}$	$(4.86\pm0.26)\times10^{-2}$	$(8.80\pm0.38)\times10^{-3}$	$(9.90\pm0.10)\times10^{-3}$
Fe^{55} Parallel CTI[(iii)]	$(5.14\pm3.90)\times10^{-6}$	$(4.05\pm0.54)\times10^{-5}$	$(1.23\pm0.59)\times10^{-6}$	$(3.07\pm0.08)\times10^{-5}$
Fe^{55} Serial CTI: (Standard register)	$(1.05\pm1.36)\times10^{-6}$	$(2.04\pm2.66)\times10^{-6}$	$(1.73\pm1.49)\times10^{-6}$	$(1.08\pm0.67)\times10^{-5}$
Fe^{55} Serial CTI: (EM register)	$(1.19\pm0.01)\times10^{-4}$	$(6.82\pm0.01)\times10^{-4}$	$(1.69\pm0.01)\times10^{-4}$	$(1.83\pm0.01)\times10^{-4}$

[(i)] Reported values were measured using the Rϕ2HV values in Table 2 and ϕDC = 5 V.
[(ii)] Measured at default datasheet voltages[7]
[(iii)] X-ray CTI measured using an integration time of 100s, using an X-ray density of ≈ 1 X-ray per 200 pixels.
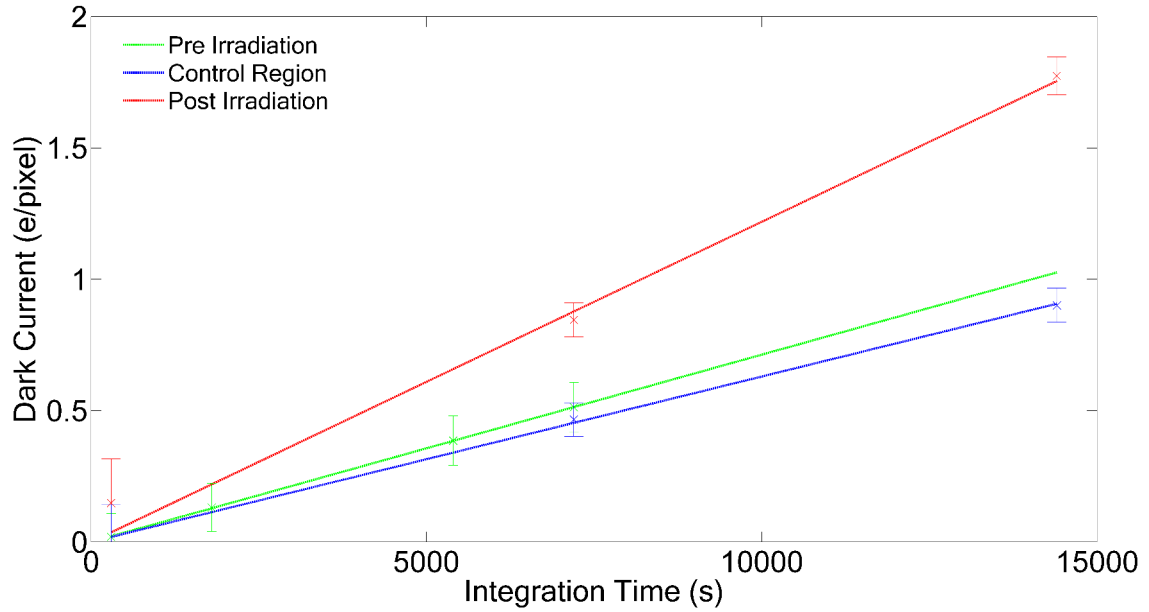
Figure 7: Dark current measured for device 1 pre- and post-irradiation. The measured values pre-irradiation and for the control region post-irradiation agree within error, as expected. The dark current within the irradiated region increased by approximately a factor of 2
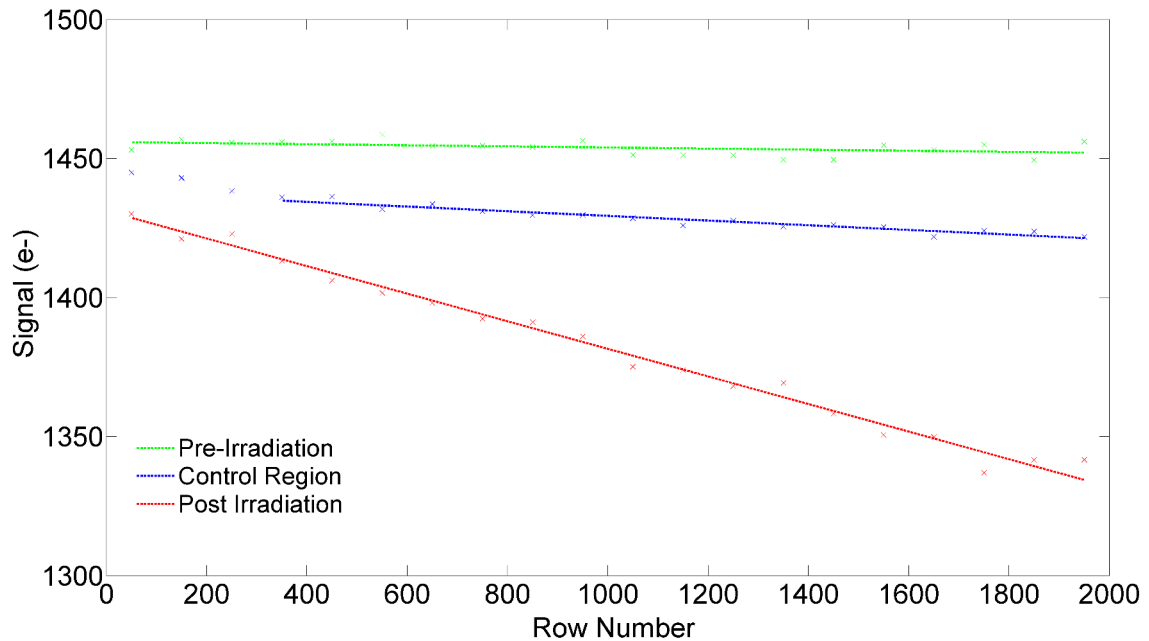

Figure 8: Parallel X-ray CTI for device 2 pre- and post-irradiation. The intercept is not $1616e^-$ as would normally be expected since some of the charge was deferred by the EM register (section 4.4). To ensure the serial register of this device was irradiated the entire parallel section of the device was irradiated across $\approx$300 rows (figure 5). The effect can be seen for the first 300 rows of the control region data, where a similar gradient to the irradiated region is present.
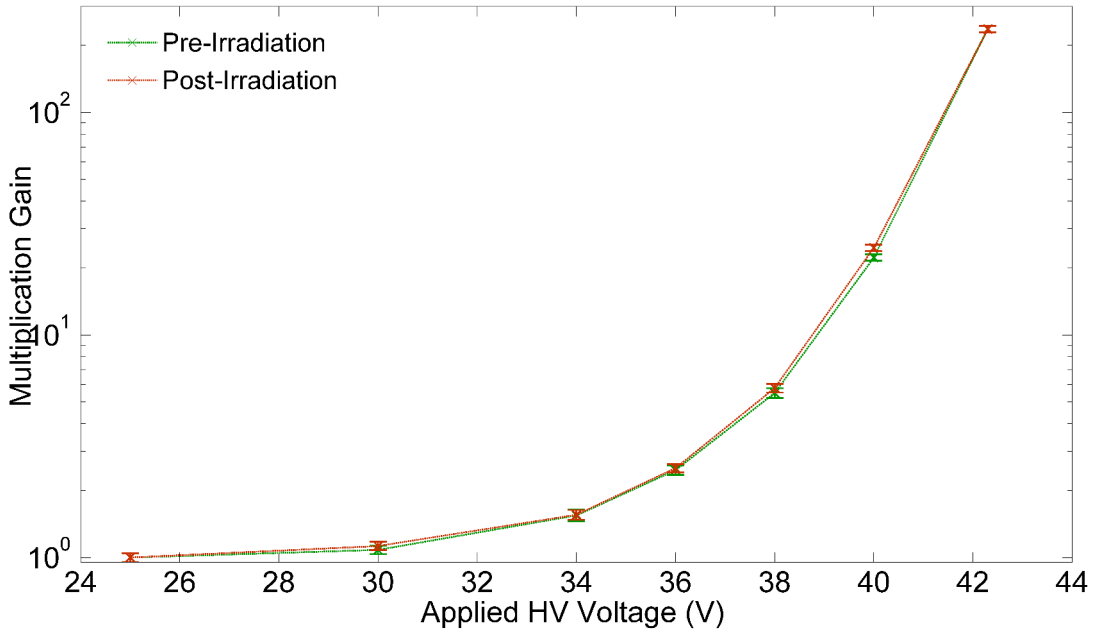
Figure 9: Multiplication Gain measured for device 2 pre- and post-irradiation. The measured values agreed within error for the Rϕ2HV values used in this study

5. CONCLUSIONS AND FUTURE WORK

In summary, the results of this initial investigation into the effects of displacement damage on the CCD201-20 are very encouraging. The multiplication gain was unchanged by irradiation and the dark current increase for these devices appears consistent at approximately $\times 2$. Parallel CIC showed no significant change and the values shown will be minimised further through operation at faster pixel rates and with optimised clocking waveforms. The degradation of X-ray CTI has followed the expected trend in both parallel and serial directions, however further work is required to fully understand how this will impact the AFTA-C application and to determine if the degradation can be mitigated through optimizing the readout schemes.

Although this investigation was very successful, further work is required to fully understand the effects of radiation damage on the CCD201-20. The conditions for which the device will experience radiation throughout the mission lifetime are different to what the devices were exposed to for this particular study. The device will be both biased and at its nominal operating temperature, which are each expected to affect how radiation damage manifests into performance degradation for the device. Future work will therefore entail a clocked and biased, cryogenic irradiation of the CCD201-20 in order to further investigate the differences in degradation that can be expected when compared to the room temperature irradiation described in this study.

The irradiation will be performed at the Helios-3 beamline at Harwell, U.K and will make use of custom designed equipment described by Gow *et al.*[31] so that the device can be attached and removed from the beamline during the pre- and post-irradiation characterisation tests. A total of four separate fluences will be applied to the device, with tests similar to those described in this study being performed between each successive fluence. Following the final irradiation, the device will experience a short room temperature anneal before a final post-irradiation characterisation takes place. Specific attention will be paid to the annealing process and its effect on dark current and CTI, as this will inform whether an on-board anneal during the mission would be beneficial to the instrument.

Moving forwards, it may be possible to use the technique of trap-pumping to characterise the different trap species present within the devices following irradiation.[32,33,34,35] The trap parameters derived through trap-

13

pumping can be used to guide modelling of charge transfer and help to develop correction strategies.[36] Before applying correction techniques, however, the devices should be fully optimised and the use of novel operating techniques considered to improve the intrinsic device performance following irradiation.[37,17] The results from the future planned cryogenic irradiation investigation, alongside possible mitigation techniques, shall provide further insight into the effects if displacement damage on the CCD201-20 and how the device can be optimised for the AFTA-C mission.

REFERENCES

[1] Dressing, C. D. and Charbonneau, D., "The occurrence of potentially habitable planets orbiting m dwarfs estimated from the full kepler dataset and an empirical measurement of the detection sensitivity," **807**, 45 (July 2015).

[2] Batalha, N. M., Rowe, J. F., and Bryson, S. T. e. a., "Planetary candidates observed by kepler. iii. analysis of the first 16 months of data," **204**, 24 (Feb. 2013).

[3] Walker, G. A. H., "The first high-precision radial velocity search for extra-solar planets," **56**, 9–15 (Jan. 2012).

[4] Kipping, D. M., Torres, G., Buchhave, L. A., Kenyon, S. J., Henze, C., Isaacson, H., Kolbl, R., Marcy, G. W., Bryson, S. T., Stassun, K., and Bastien, F., "Discovery of a transiting planet near the snow-line," **795**, 25 (Nov. 2014).

[5] Spergel, D., Gehrels, N., and et al., B., "Wide-Field InfrarRed Survey Telescope-Astrophysics Focused Telescope Assets WFIRST-AFTA 2015 Report," *ArXiv e-prints* (Mar. 2015).

[6] Jerram, P., Pool, P. J., Bell, R., and Burt, D. J. e. a., "The llccd: low-light imaging without the need for an intensifier," *Proc. SPIE* **4306**, 178–186 (2001).

[7] e2v technologies, "e2v ccd201-20 datasheet,"

[8] Heim, G. B., Burkepile, J., and Frame, W. W., "Low-light-level emccd color camera," *Proc. SPIE* **6209**, 62090F–62090F–11 (2006).

[9] Teo, B K; Shestakova, I. S. M. B. W. C. N. V. V. . H. B. H., "Evaluation of a emccd detector for emission-transmission computed tomography.," *IEEE Transactions on Nuclear Science* **53**(5), 2495–2499 (2006).

[10] Mackay, C., Staley, T. D., King, D., Suess, F., and Weller, K., "High-speed, photon-counting CCD cameras for astronomy," in [*Society of Photo-Optical Instrumentation Engineers (SPIE) Conference Series*], *Society of Photo-Optical Instrumentation Engineers (SPIE) Conference Series* **7742**, 2 (July 2010).

[11] Harding, L., Demers, R., and Hoenk, M. e. a., "Technology advancement of the ccd201-20 emccd for the wfirst-afta coronagraph instrument: sensor characterization and radiation damage (accepted for publication with minor corrections)," *JATIS* (July 2015).

[12] Robbins, M. S. and Hadwen, B. J., "The noise performance of electron multiplying charge-coupled devices," *Electron Devices, IEEE Transactions on* **50**(5), 1227–1232 (2003).

[13] Tutt, J. H., Holland, A. D., Hall, D. J., Harriss, R. D., and Murray, N. J., "The noise performance of electron-multiplying charge-coupled devices at x-ray energies," *Electron Devices, IEEE Transactions on* **59**(1), 167–175 (2012).

[14] Basden, A. G., Haniff, C. A., and Mackay, C. D., "Photon counting strategies with low-light-level ccds," **345**, 985–991 (Nov. 2003).

[15] Daigle, O. and Blais-Ouellette, S., "Photon counting with an emccd," *Proc. SPIE* **7536**, 753606–753606–10 (2010).

[16] Daigle, O., Gach, J.-L., Guillaume, C., Lessard, S., Carignan, C., and Blais-Ouellette, S., "CCCP: a CCD controller for counting photons," in [*Society of Photo-Optical Instrumentation Engineers (SPIE) Conference Series*], *Society of Photo-Optical Instrumentation Engineers (SPIE) Conference Series* **7014**, 6 (July 2008).

[17] Murray, N. J., Burt, D. J., Holland, A. D., Stefanov, K. D., Gow, J. P., MacCormick, C., Dryer, B. J., and Allanwood, E. A., "Multi-level parallel clocking of ccds for: improving charge transfer efficiency, clearing persistence, clocked anti-blooming, and generating low-noise backgrounds for pumping," in [*SPIE Optical Engineering+ Applications*], 88600K–88600K, International Society for Optics and Photonics (2013).

[18] Daigle, O., Gach, J.-L., Guillaume, C., Lessard, S., Carignan, C., and Blais-Ouellette, S., "CCCP: a CCD controller for counting photons," in [*Society of Photo-Optical Instrumentation Engineers (SPIE) Conference Series*], *Society of Photo-Optical Instrumentation Engineers (SPIE) Conference Series* **7014**, 6 (July 2008).

[19] Smith, D. R., Ingley, R., and Holland, A. D., "Proton irradiation of emccds," *Electron Devices, IEEE Transactions on* **53**(2), 205–210 (2006).

[20] "The effects of co^{60} gamma radiation on electron multiplying charge-coupled devices," *IEEE Transactions on Nuclear Science* **51**(05), 2747–2752 (2004).

[21] e2v technologies, "e2v ccd-97 datasheet,"

[22] Evagora, A., Murray, N., Holland, A., and Burt, D., "Single event gate rupture in emccd technology," *Journal of Instrumentation* **7**(12), C12002 (2012).

[23] Burke, E. et al., "Energy dependence of proton-induced displacement damage in silicon," *Nuclear Science, IEEE Transactions on* **33**(6), 1276–1281 (1986).

[24] Van Lint, V. A., "The physics of radiation damage in particle detectors," *Nuclear Instruments and Methods in Physics Research Section A: Accelerators, Spectrometers, Detectors and Associated Equipment* **253**(3), 453–459 (1987).

[25] Srour, J., Marshall, C. J., and Marshall, P. W., "Review of displacement damage effects in silicon devices," *Nuclear Science, IEEE Transactions on* **50**(3), 653–670 (2003).

[26] Evagora, A., Murray, N., Holland, A., Burt, D., and Endicott, J., "Novel method for identifying the cause of inherent ageing in electron multiplying charge coupled devices," *Journal of Instrumentation* **7**(01), C01023 (2012).

[27] Bush, N., Stefanov, K., Hall, D., Jordan, D., and Holland, A., "Simulations of charge transfer in electron multiplying charge coupled devices," *Journal of Instrumentation* **9**(12), C12042 (2014).

[28] "Assessment of space proton radiation-induced charge transfer inefficiency in the ccd204 for the euclid space observatory," *JINST* **7**(01), C01030 (2012).

[29] Daigle, O., Djazovski, O., Francoeur, M., Laurin, D. G., and Doyon, R., "Emccds: 10 mhz and beyond," in [*SPIE Astronomical Telescopes+ Instrumentation*], 91540B–91540B, International Society for Optics and Photonics (2014).

[30] Daigle, O., Carignan, C., Gach, J.-L., Guillaume, C., Lessard, S., Fortin, C.-A., and Blais-Ouellette, S., "Extreme Faint Flux Imaging with an EMCCD," **121**, 866–884 (Aug. 2009).

[31] Gow, J. P. D., Smith, P. H., Pool, P., Hall, D. J., Holland, A. D., and Murray, N. J., "Proton irradiation of a swept charge device at cryogenic temperature and the subsequent annealing," *Journal of Instrumentation* **10**(01), C01037 (2015).

[32] Murray, N., Holland, A., Gow, J., Hall, D., Tutt, J. H., Burt, D., and Endicott, J., "Mitigating radiation-induced charge transfer inefficiency in full-frame ccd applications by pumpingtraps," (2012).

[33] Murray, N. J., Burt, D. J., Hall, D., and Holland, A. D., "The relationship between pumped traps and signal loss in buried channel ccds," in [*SPIE Optical Engineering+ Applications*], 88600H–88600H, International Society for Optics and Photonics (2013).

[34] Hall, D. J., Murray, N. J., Holland, A. D., Gow, J., Clarke, A., and Burt, D., "Determination of in situ trap properties in ccds using a single-trap pumping technique," *Nuclear Science, IEEE Transactions on* **61**(4), 1826–1833 (2014).

[35] Hall, D. J., Murray, N., Gow, J., Wood, D., and Holland, A., "In situ trap parameter studies in ccds for space applications," in [*SPIE Astronomical Telescopes+ Instrumentation*], 915408–915408, International Society for Optics and Photonics (2014).

[36] Hall, D. J., Holland, A., Murray, N., Gow, J., and Clarke, A., "Modelling charge transfer in a radiation damaged charge coupled device for euclid," in [*SPIE Astronomical Telescopes+ Instrumentation*], 845315–845315, International Society for Optics and Photonics (2012).

[37] Hall, D. J., Gow, J., Murray, N. J., and Holland, A. D., "Optimization of device clocking schemes to minimize the effects of radiation damage in charge-coupled devices," *Electron Devices, IEEE Transactions on* **59**(4), 1099–1106 (2012).